



Measurement of magnetic fields and creating their respective heatmaps

P&S: MAGNETIC FIELDS IN DAILY LIFE

Presented by: Enrique Baltis, Elia Martin, Akshayan Nanthakumaran

Supervised by: Marco Zahner

December 2025

Contents

1	Introduction	3
2	Theory & Setup	3
2.1	Physical Fundamentals of Magnetic Fields	3
2.2	Sensor Physics and The Hall Effect	3
2.3	Kinematic Integration and Drift	4
2.4	Methods of Measurement	4
2.4.1	Expom-Elf Magnetometer	4
2.4.2	Ultrasonic Sensor with Arduino	4
2.4.3	Auto Magnetic Sensor with position tracking	5
2.5	Macro vs Micro	6
3	Measurement and Results	8
3.1	Table ETZ	8
3.2	Table in Barn	9
3.3	Table in Barn with Magnet	11
3.4	Experimenting with the limitations	12
3.4.1	Measurement with Offset	12
3.4.2	Varying measurement time	13
4	Summary and Conclusion	13
5	References	14

1 Introduction

Magnetic fields are an omnipresent component of the modern urban environment, coming from both natural geomagnetic sources and anthropogenic sources such as power grids, electronic devices, and structural steel. Understanding the spatial distribution and intensity of these fields is crucial for both technical applications and environmental assessments.

The primary motivation for this project was to investigate and compare various methodologies for localized magnetic field measurement and surface characterization through heatmap generation in order to better visualize the fields around us. By evaluating different sensor setups, we sought to determine how effectively fields can be mapped across common surfaces and structural transitions.

This report explores three distinct measurement approaches: the high-precision but labor-intensive manual grid-based method using the Expom-Elf magnetometer, an automated tracking system utilizing ultrasonic sensors and an Arduino microcontroller, and an inertial navigation approach based on smartphone accelerometer data. Each method was tested across diverse environments.

The report is structured as follows: Section 2 establishes the physical fundamentals and details the experimental apparatus; Section 3 presents the comparative results and generated heatmaps for each measurement subject; and Section 4 summarizes our findings regarding the optimal balance between measurement efficiency and spatial integrity. Through this work, we demonstrate the practical characterizing of magnetic topographies in our daily environment.

2 Theory & Setup

The characterization of magnetic fields in residential and laboratory environments requires an understanding of both the physical nature of the fields and the mathematical constraints of the sensors used to measure them.

2.1 Physical Fundamentals of Magnetic Fields

The magnetic field is a vector field, denoted as \vec{B} , representing the magnetic flux density. In ambient environments, we measure the magnitude B in units of micro-Tesla (μT). The total observed field at any point \vec{r} is the vector sum of the Earth's geomagnetic field \vec{B}_{geo} and localized perturbations \vec{B}_{loc} :

$$\vec{B}_{total}(\vec{r}) = \vec{B}_{geo} + \vec{B}_{loc}(\vec{r})$$

Localized fields produced by ferromagnetic "micro" sources often behave as magnetic dipoles, where the intensity B decreases following the inverse-cube law $B(r) \propto 1/r^3$. This explains the high spatial gradients observed near structural elements.

2.2 Sensor Physics and The Hall Effect

The magnetometers used in this project rely on Hall effect sensors. When a current-carrying conductor is placed in a magnetic field, the Lorentz force deflects charge carriers, creating a

measurable voltage U perpendicular to the current and the field:

$$U = R_H \frac{I \cdot B}{d}$$

where R_H is the Hall coefficient and d is the sensor thickness.

2.3 Kinematic Integration and Drift

For automated mapping using an accelerometer, position $x(t)$ is derived via double integration of acceleration $a(t)$. However, micro-electromechanical systems suffer from additive noise ϵ , resulting in a quadratic position error (drift) over time: $\Delta x(t) = \frac{1}{2}\epsilon t^2$. Drift compensation techniques, such as Zero-Velocity Updates, are required to maintain spatial integrity.

2.4 Methods of Measurement

2.4.1 Expom-Elf Magnetometer



Figure 1: Expom-Elf Magnetometer Setup

The Expom-Elf sensor represents a high-precision manual approach. It requires the operator to move the sensor across a predefined grid, allowing the reading to stabilize at each measurement interval. While this method ensures reliable data and simplifies analysis, it is time-intensive and cannot be largely streamlined for large-scale mapping.

2.4.2 Ultrasonic Sensor with Arduino

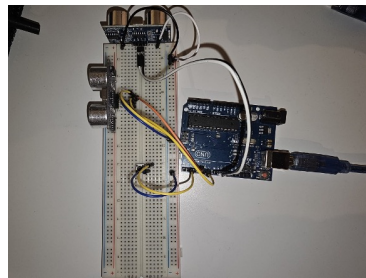


Figure 2: Arduino setup

To automate position-tracking and improve spatial resolution, ultrasonic distance sensors were integrated into the measurement apparatus. For controlling the ultrasound sensors, an Arduino UNO board was used, as well as a smartphone to measure the magnetic field running Phyphox. The measurement procedure involved coupling the phone with the sensors on a protoboard (also known as a breadboard), starting them simultaneously, and smoothly traversing the setup across the desired measurement object. The Arduino output consists of a timestamp and 2 ultrasound sensor readings. The phone output consists of magnetic field readings, which would then be synchronized with the magnetic field data by correlating timestamps between the Arduino and the smartphone.

This method generates a map with a discrete set of data points, each with a magnetic field value. This is then spread across the whole map using an interpolation algorithm in order to generate a more continuous heat map. This post-measurement work posed some difficulty, as the distance measurements were not flawless and sometimes the path of the setup needed to be corrected.

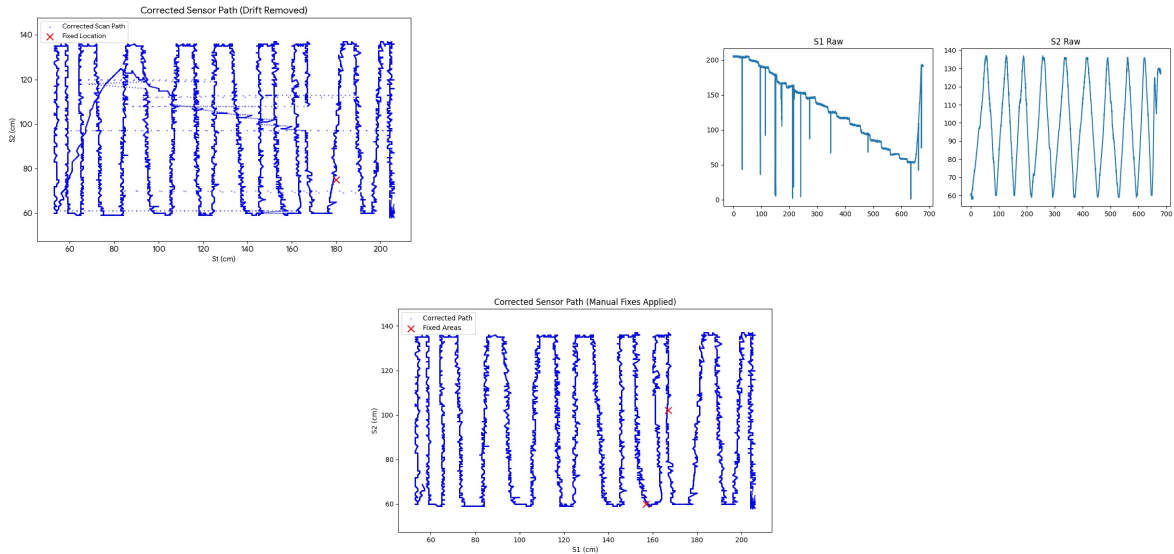


Figure 3: Process of cleaning up a path

2.4.3 Auto Magnetic Sensor with position tracking

We further investigated position tracking using a smartphone's internal accelerometer. This method is theoretically achievable by integrating the acceleration graph twice. However, double integration of acceleration data is susceptible to cumulative errors, making it impractical for complex paths or extended durations. Our strategy to solve this was two-fold:

1. **Signal De-Noising:** In order to filter out the noise from the accelerometer, a low-pass filter was applied in software, i.e. higher frequencies (> 2 Hz) would be set to zero in the spectral graph. Another front for this strategy was to set small velocities arising from false non-zero accelerations to zero.
2. **Drift Compensation:** Over time, the acceleration values kept rising in a linear manner, something that proved to be the biggest downside to this method. To try mitigating this, we imposed 2 additional conditions, start/end position and velocity. For closed-loop paths,

we imposed that the path should start and end at the same spot and that the phone was at rest in both moments.

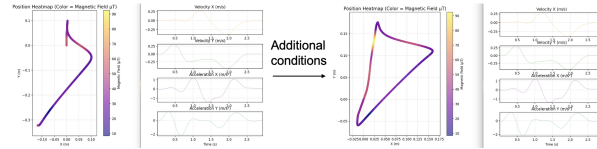


Figure 4: Implementation of additional conditions

Even though the employed fixes were effective, for longer measurements the data manipulation required excessive post-processing. Consequently, we settled on a practical "straight-line" approach, splicing multiple linear measurements into a single unified heatmap. This approach, though fast when measuring, proved to be more taxing on the post-measurement analysis.

2.5 Macro vs Micro

We did several measurements to show the difference between macro and micro.

Macro refers mostly to the static magnetic field of the Earth combined with large ferromagnetic structures, e.g. steel, ferroconcrete, etc. The field is generally uniform over small distances, especially if there is no ferromagnetic structure nearby, as the maximum regional gradient across Switzerland is approximately $1.25 \mu\text{T}$ [1]. Therefore, the gradient is low and smooth. When adding ferromagnetic structures, the spectrum can change rapidly, especially if one is near the structure. However, it is generally quite difficult to identify the correct influencing variable.

Micro-scale measurements utilize the ambient geomagnetic field as a baseline, but exhibit significant localized deviations due to nearby dipoles. Small movements can yield large discrepancies due to the inverse cube law, so the gradient is steep and sharp. Due to this, it is much easier to identify the influence.

Macro-Measurements: Inside a house

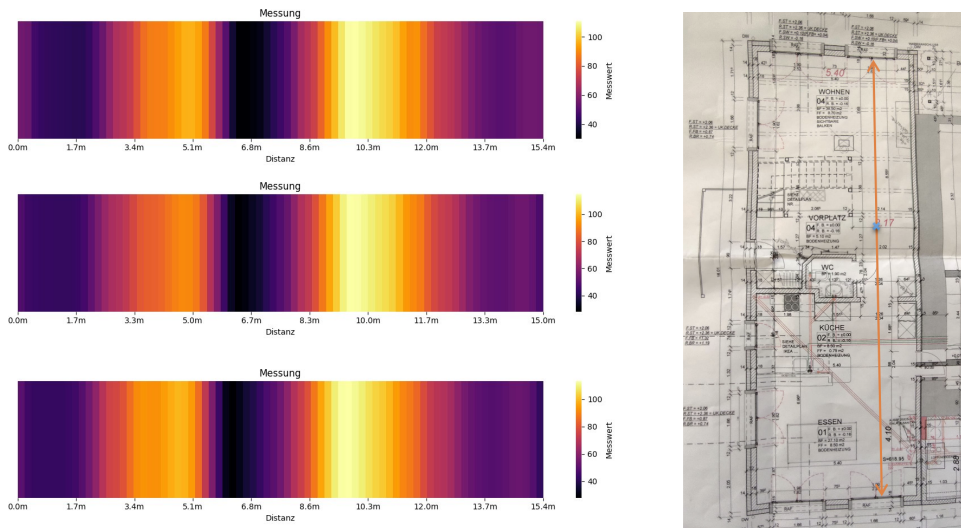


Figure 5: Comparison: Three individual measurements (Left) vs. house floor-plan and the path in orange (Right)

These measurements were done on different days at different times, with a standard deviation of $0.763 \mu\text{T}$. Therefore, even though the power consumption in the house was different at each measurement, there was little to no impact on the magnetic field (ferro metallic structures seem to overrule). As per floor-plan, there is no clear indicator why the peak (blue cross) would be where it is.

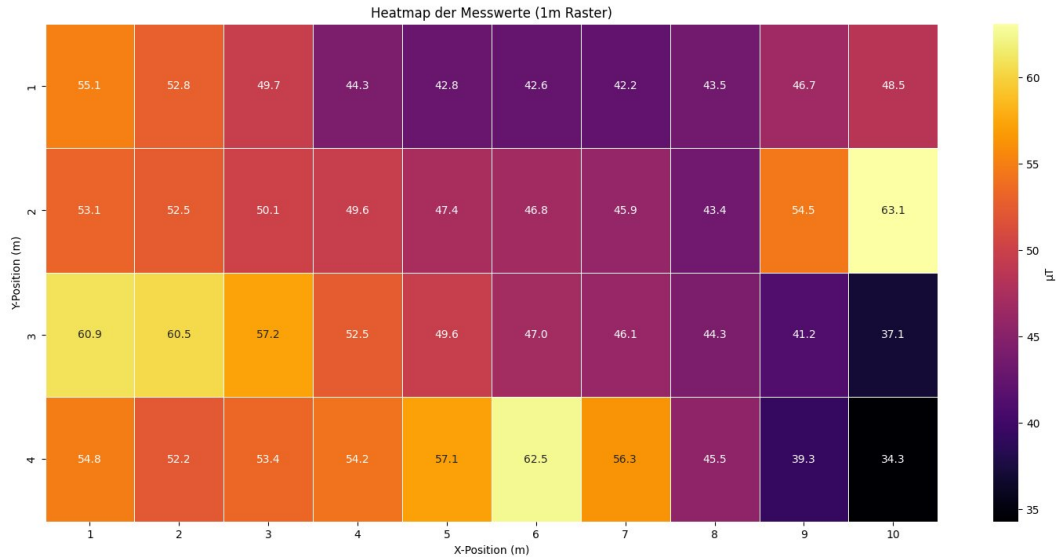


Figure 6: Measurements inside a house

In the heatmap above there is a wall on the left, a garden on the right and then entertainment systems, such as TV, Playstation, etc. These results confirm that localized structural influences predominate over transient electronic noise in residential environments.

Difference between inside and outside

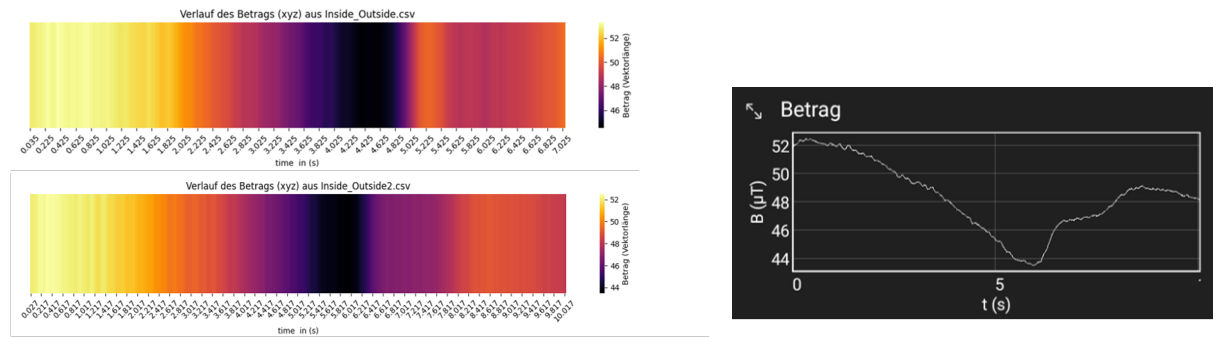


Figure 7: Comparison: Two individual measurements (Left) and a measurement as a graph (Right). The transition goes from the inside to outside

The gradient in the inside and outside transition is rather small. This is due to the reinforced concrete and cables in the walls, which weaken the magnetic field.

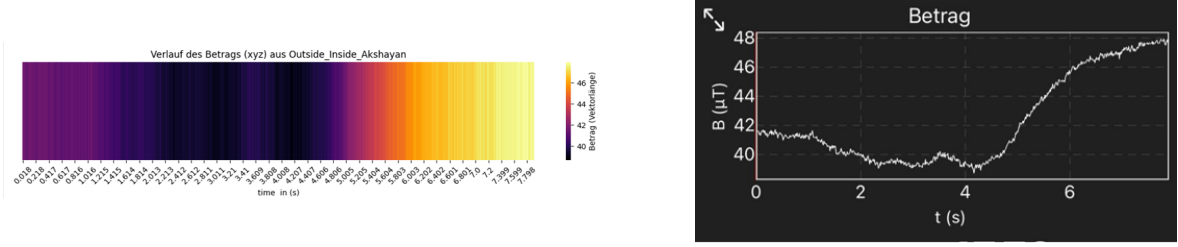


Figure 8: Comparison: Measurement in another house (Left) and the measurement as a graph (Right). The transition goes from the outside to inside

3 Measurement and Results

Two tables were selected as measurement subjects to provide a controlled, stable, and flat surface environment, minimizing geometric variables. A comparative analysis was conducted by applying all three measurement techniques to each experimental setup. The manual Expom-Elf heatmap provided the baseline for accuracy. This was compared against the automated ultrasonic heatmap and the inertial accelerometer method.

3.1 Table ETZ

The first measurement series was conducted on a table in a ETZ room. The manual Expom-Elf measurement established a high-resolution baseline, revealing a complex magnetic topology likely influenced by the table's internal steel supports and proximity to magnets.

When comparing the results, the ultrasonic-tracked setup (Fig. 10) successfully captured the general flux density distribution, though the raw data exhibited spatial jitter due to ultrasonic reflections. However, after applying the interpolation algorithm (Fig. 11), the generated heatmap showed strong alignment with the manual baseline.

The accelerometer-based method proved the most efficient for rapid data acquisition, in other words for "prototyping". By capturing seven parallel linear strips, each taking about 1.5 seconds, we were able to reconstruct the full magnetic flux density across the table's surface. As shown in Figure 12, this method effectively visualized the steep gradients between the table's structural components, confirming that the straight-line mapping approach provides a reliable balance between spatial resolution and temporal efficiency.

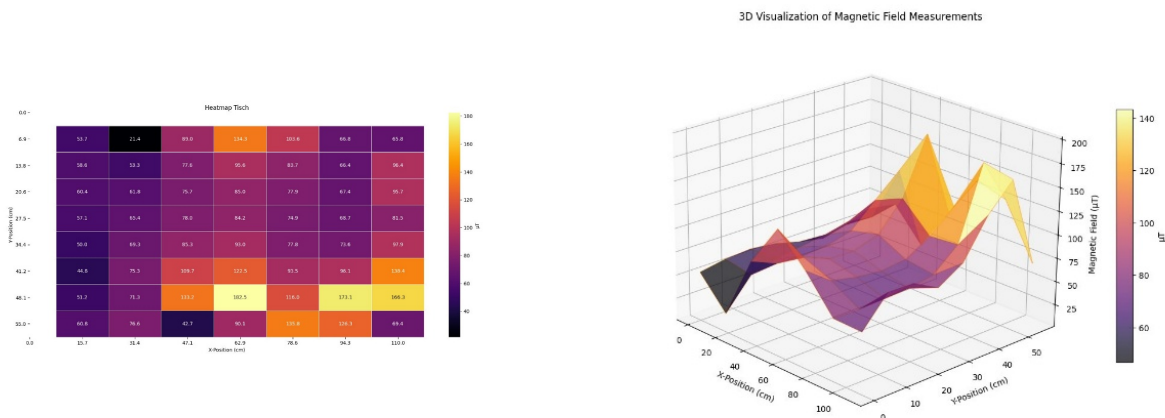


Figure 9: Expom-Elf Heatmap of the ETZ Table

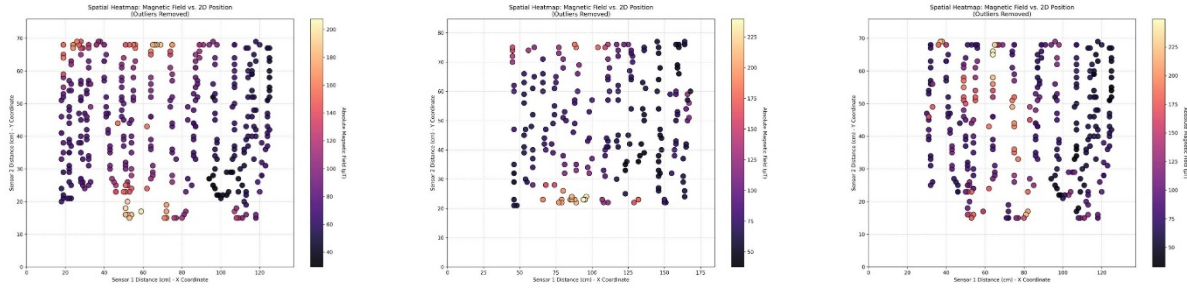


Figure 10: Heatmap of the ETZ Table with ultrasonic sensors

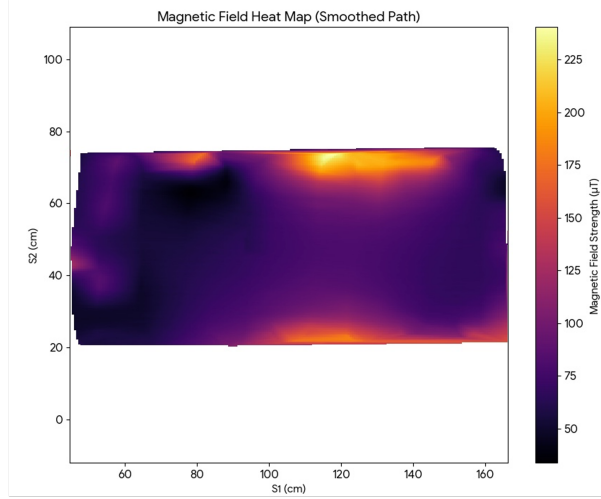


Figure 11: Interpolated Heatmap of the ETZ Table

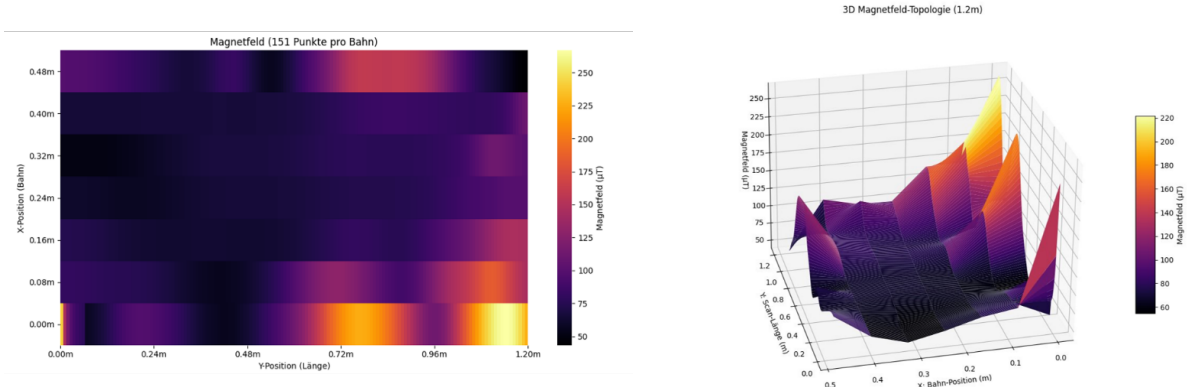


Figure 12: Measurements with only accelerometer

Before having done these measurements, the expectation would have been that the table's magnetic topography was symmetrical, however, it clearly is not. This could be due to a multitude of reasons, e.g. deformity of the table legs/metal bars, magnetization of the metal parts by leaving magnets on them and so on.

3.2 Table in Barn

For the second table, we moved our location, as we were not sure if there was some external influence on the magnetic field of the table in the ETZ. The barn, as opposed to the ETZ building,

was constructed entirely out of wood and contained virtually no ferromagnetic materials. This ensured data integrity, free from external ferromagnetic interference.



Figure 13: Table setup in the barn

The measurements yielded:

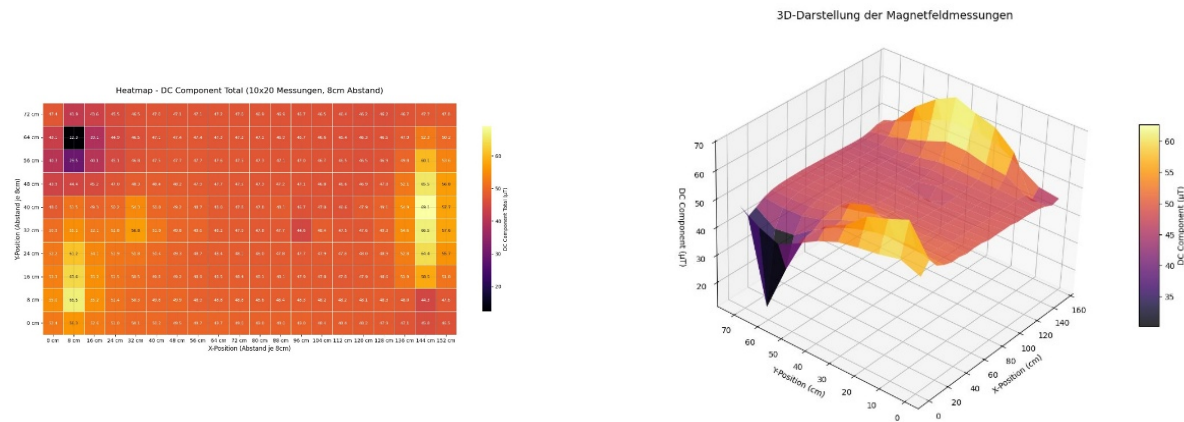


Figure 14: Expom-Elf Heatmap of the barn Table

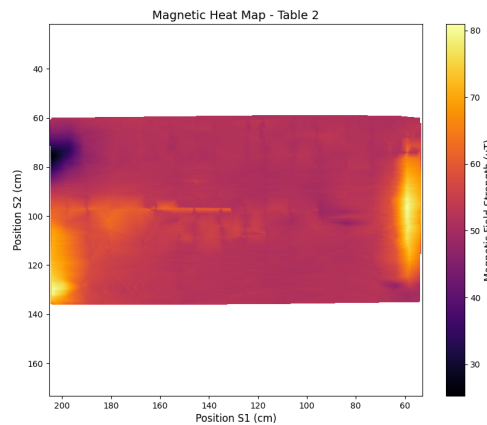
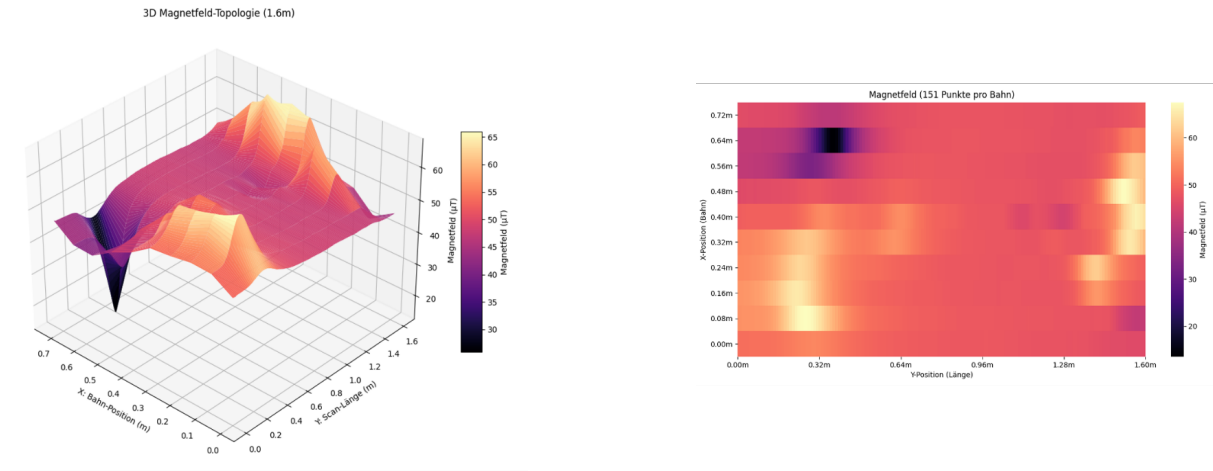


Figure 15: Heatmap of the barn Table with ultrasonic sensors

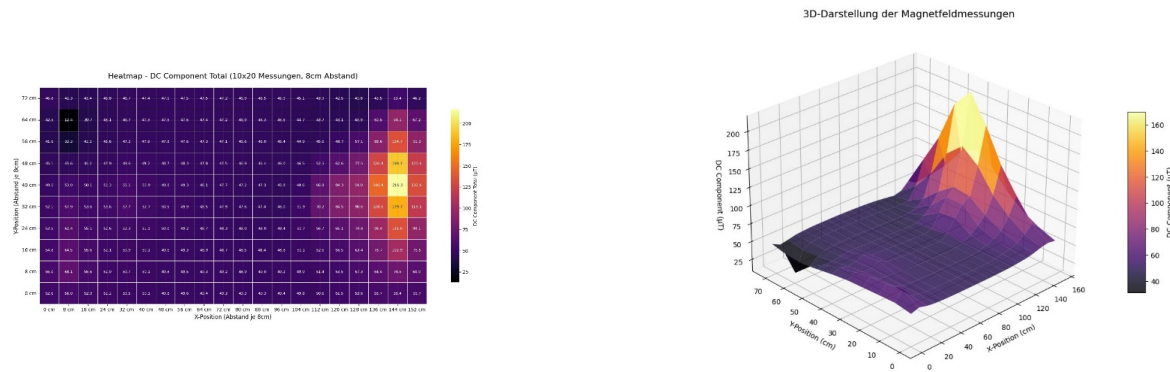
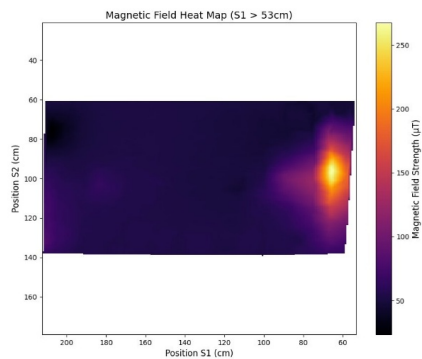
Note the yellow horizontal strip in the middle of the table. This comes from the still erroneous path registered by the ultrasound sensors, leading values from someplace else to be "carried over".

**Figure 16:** Heatmap of the barn Table using accelerometer

There is a recognizable asymmetry. One side has both legs with the same magnetic fields, forming a "pyramid". However, the opposite side is almost antisymmetric, with a higher and a lower side. Probable cause is the distance difference from the metal bars to the table, as it can be seen in Fig 13, something to be expected because of the magnetic field's inverse cube law.

3.3 Table in Barn with Magnet

We introduced a magnet to a table leg to observe local dipole effects.

**Figure 17:** Expom-Elf Heatmap of the barn Table with an added magnet**Figure 18:** Heatmap of the barn Table with an added magnet with ultrasonic sensors

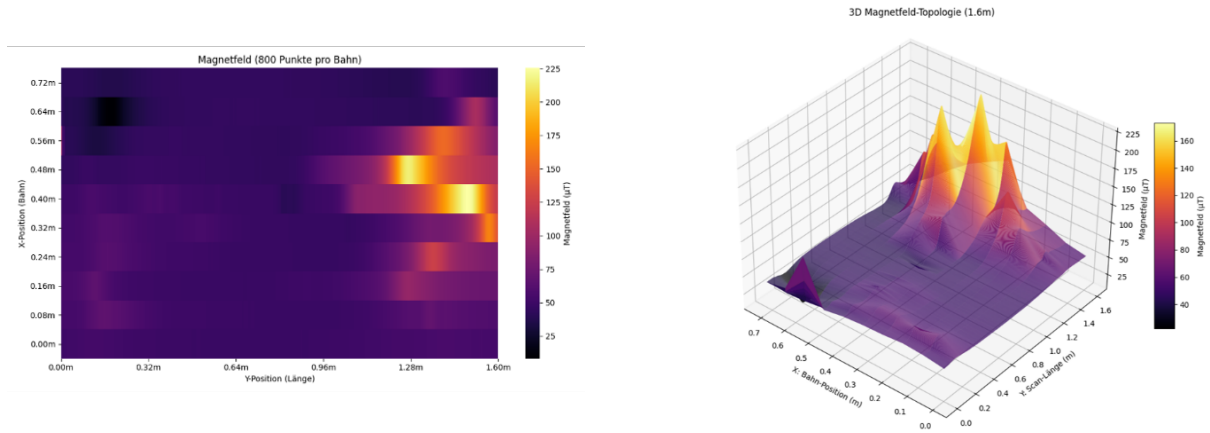


Figure 19: Heatmap of the barn Table using accelerometer

What these measurements showed was that the introduction of a strong magnet diminishes the influence of the static metallic structures on the surface. As it is clearly visible, the majority of the map presents a similar colour, except for where the magnet was placed.

3.4 Experimenting with the limitations

Even though all three methods performed well, we still wanted to test them in more extreme conditions, such as with shorter measurement times and exposing the sensors to high magnetic fields.

3.4.1 Measurement with Offset

At some point when measuring with the accelerometer via phyphox, the smartphone came close to the magnet and got a significant offset. This is clearly visible on the 3D-Heatmap, when the smartphone sensor approached the saturation threshold of the local dipole, resulting in a measurement spike exceeding five times the predicted intensity.

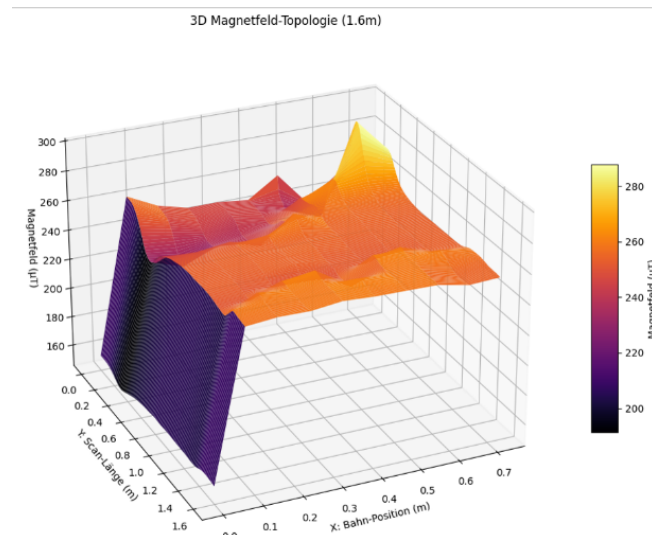


Figure 20: Measurement error due to sensor offset

3.4.2 Varying measurement time

We tested for the methods with ultrasound and accelerometer.

Ultrasonic sensors:

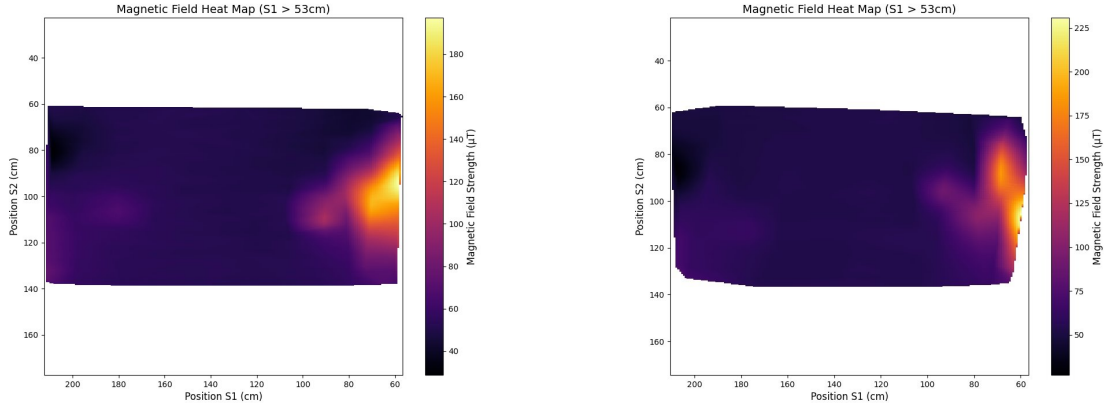


Figure 21: 30 seconds long measurement vs. 10 seconds long measurement

This clearly shows that even with less data points, the resulting maps still generate a reasonable representation of a surface.

Accelerometer:

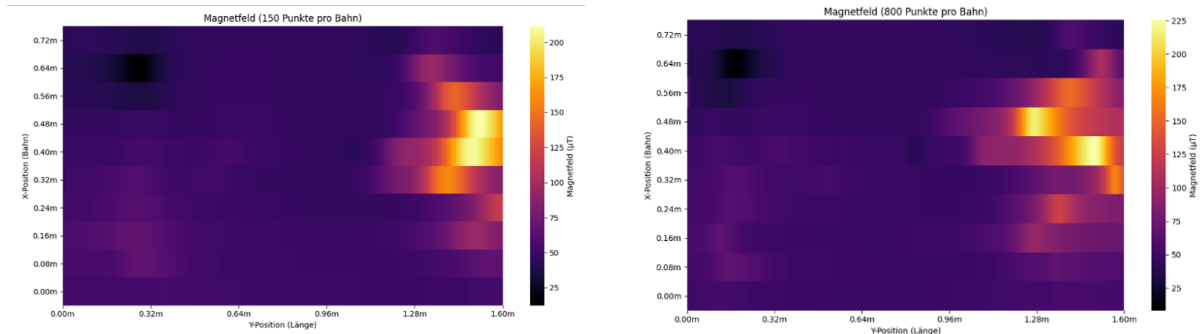


Figure 22: 1.5 seconds per strip vs. 8 seconds per strip

This shows the main downside of measurements using accelerometers, which is the drift over time, i.e., the longer the measurement time, the less accurate the position tracking is. However, both still generated similar maps.

4 Summary and Conclusion

Table 1: Quantitative Comparison of Magnetic Field Mapping Methodologies

Method	Precision	Efficiency	Ease of Setup	Primary Limitation
Expom-Elf	High (Baseline)	Very Low	High	Manual grid
Ultrasonic	Medium	Medium	Medium	Signal jitter; path errors
Accelerometer	Low (Drift)	High	High	Quadratic position drift

This study investigated three distinct methodologies for mapping magnetic field distributions and characterizing surfaces through heatmap generation. By conducting a comparative analysis of manual grid-based magnetometry, automated ultrasonic tracking, and smartphone-based inertial navigation, we identified the primary trade-offs between acquisition efficiency and spatial accuracy.

Our findings indicate that, while the manual Expom-Elf method remains the benchmark for absolute precision, automated systems offer a significant advantage in temporal efficiency for large-area mapping. The integrated Arduino-ultrasound apparatus and the drift-compensated accelerometer method successfully captured localized magnetic gradients, such as the high-intensity fields around structural dipoles, which were then visualized through continuous interpolation heatmaps. Furthermore, we demonstrated the effective use of digital signal processing, specifically low-pass filtering and kinematic boundary constraints, to neutralize sensor drift and noise inherent in mobile measurement platforms.

Ultimately, this work concludes that an automated hybrid measurement approach provides the most robust solution for characterizing complex magnetic topographies in daily life. Future projects should explore fusion of both the accelerometer and ultrasound data to further reduce spatial uncertainty and facilitate the mapping of non-linear measurement trajectories. The code and data used to plot our graphs are available on GitHub [2].

5 References

References

- [1] swisstopo. Total intensity - geophysics, 2025. Accessed: 2025-12-25.
- [2] Enrique Baltis, Elia Martin, and Akshayan Nanthakumaran. Project code. https://github.com/heinrichsemj/PS_magfield/, 2025.